UNIVERSIDAD REGIONAL AMAZÓNICA IKIAM

FACULTAD DE CIENCIAS DE LA TIERRA Y AGUA

CARRERA EN GEOCIENCIAS

Proyecto de investigación previo a la obtención del título de Ingeniero en Geociencias

ANÁLISIS DE ESTABILIDAD DE TALUDES ROCOSOS, EN UN TRAMO DE LA VÍA TENA – BAEZA, REGIÓN SUBANDINA DEL ECUADOR

Autor: Anderson David Ocampos Valarezo

Tutor: Jorge Ronny Espín Campos

Tena, Diciembre 2021

UNIVERSIDAD REGIONAL AMAZÓNICA IKIAM

Facultad de Ciencias de la Tierra y Agua

Ingeniería en Geociencias

Análisis de Estabilidad de Taludes Rocosos, en un tramo de la vía Tena – Baeza, Región Subandina del Ecuador

Anderson David Ocampos Valarezo

14 de septiembre de 2021, ciudad de Tena, Napo, Ecuador

DECLARACIÓN DE DERECHO DE AUTOR, AUTENTICIDAD Y RESPONSABILIDAD

Tena, 14 de septiembre del 2021

Yo, Anderson David Ocampos Valarezo con documento de identidad N° 150094054-7, declaro que los resultados obtenidos en la investigación que presento en este documento final, previo a la obtención del título de Ingeniero en Geociencias son absolutamente inéditos, originales, auténticos y personales.

En virtud de lo cual, el contenido, criterios, opiniones, resultados, análisis, interpretaciones, conclusiones, recomendaciones y todos los demás aspectos vertidos en la presente investigación son de mi autoría y de mi absoluta responsabilidad.

Por la favorable atención a la presente, suscribo de usted,

Atentamente,

Firma:

_____

Anderson David Ocampos Valarezo
150094054-7

INVESTIGACIÓN | Parroquia Muyuna, kilómetro 7 vía a Alto Tena
INNOVACIÓN | Tena · Napo · Ecuador
EDUCACIÓN | **Telf.:** (06) 370 0040 · (06) 299 9160

www.ikiam.edu.ec
@u_ikiam IkiamOficial u_ikiam Universidad Ikiam

CERTIFICADO DE DIRECCIÓN DE TRABAJO DE INTEGRACIÓN CURRICULAR

Certifico que el trabajo de integración curricular titulado: "Análisis de Estabilidad de Taludes Rocosos, en un tramo de la vía Tena – Baeza, Región Subandina del Ecuador", en la modalidad de: proyecto de investigación en formato artículo original, fue realizado por: Anderson David Ocampos Valarezo, bajo mi dirección.

El mismo ha sido revisado en su totalidad y analizado por la herramienta de verificación de similitud de contenido; por lo tanto, cumple con los requisitos teóricos, científicos, técnicos, metodológicos y legales establecidos por la Universidad Regional Amazónica Ikiam, para su entrega y defensa.

Tena, 14 de septiembre del 2021

Firma:

Firmado electrónicamente por:
JORGE RONNY ESPIN CAMPOS

……

Jorge Ronny Espín Campos

C.I: 160048820-7

INVESTIGACIÓN | Parroquia Muyuna, kilómetro 7 vía a Alto Tena
INNOVACIÓN | Tena · Napo · Ecuador
EDUCACIÓN | Telf.: (06) 370 0040 · (06) 299 9160
www.ikiam.edu.ec
@u_ikiam IkiamOficial u_ikiam Universidad Ikiam

AGRADECIMIENTOS

Agradeceré por siempre a mi tutor de tesis Mgs. Ronny Espín por facilitarme todas las herramientas y conocimiento técnico necesario para realizar el presente trabajo de investigación de principio a fin.

También, agradecer a todos los docentes de la carrera con quienes he compartido clases presenciales y virtuales, de una u otra forma han sabido transmitir su conocimiento y entero apoyo para la formación de profesionales en Geociencias. De igual manera, agradezco a todos mis compañeros, que de buena voluntad supieron apoyarme en las jornadas de recolección de datos en campo.

Mi eterna gratitud a cada una de las personas que conforman la comunidad universitaria Ikiam. Profesores, amigos y colegas han dejado una enseñanza humana y profesional invaluable durante toda mi carrera profesional.

DEDICATORIA

En primer lugar, dedico este trabajo de investigación al conocimiento científico. Que sirva de valioso aporte en el campo de la geotécnica para el mundo y sobre todo en el Ecuador.

Dedico el presente escrito a mis queridos padres, Gladis y Néstor, por su incondicional apoyo afectivo y económico desde el inicio de mi carrera. Donde vaya, les estaré eternamente agradecido por permitirme la oportunidad de educarme académicamente y obtener un título profesional. ¡Este logro es de ustedes papitos!

También dedico este trabajo a todos mis profesores, amigos y novia que siempre estuvieron interesados en mi formación académica hasta lograr este objetivo. A todos ustedes, muchas gracias por estar presentes y compartir parte de su vida conmigo.

A todos ustedes lectores, dedico la presente investigación.

ÍNDICE GENERAL

ÍNDICE DE TABLAS

ÍNDICE DE FIGURAS

RESUMEN

Los deslizamientos en cortes viales son un problema que causa daños infraestructurales y muertes alrededor del mundo. Nosotros evaluamos la estabilidad de 14 taludes rocosos en el tramo vial Tena – Baeza. La zona de estudio se encuentra en la región Subandina del Ecuador, un área con abrupto relieve, fuertes precipitaciones y unidades litológicas ígneas y sedimentarias. Usamos dos técnicas de análisis: Análisis de Estabilidad Global en Slide 2D y Análisis Cinemático en el software Dips. Calculamos el factor de seguridad en Slide 2D usando dos métodos de Equilibrio Límite (Bishop simplificado y Spencer), y tres condiciones de saturación (seco, 50% saturado y completamente saturado). Además, condiciones pseudoestáticas fueron consideradas para tomar en cuenta la actividad sísmica en el análisis. El Análisis Cinemático se basa en datos estructurales obtenidos por brújula para determinar potenciales modos de fallo del macizo rocoso. Los resultados muestran que 11 taludes son inestables en condiciones completamente saturadas. Estos taludes tienen potenciales modos de falla tipo planar y cuña. El nivel freático saturado es el principal desencadenante de inestabilidad y la actividad sísmica no disminuye los factores de seguridad. Por otro lado, bajos valores de Índice de Resistencia Geológica indican que la meteorización y tectonismo son responsables por la pobre calidad del macizo rocoso. Para taludes globalmente inestables, recomendamos llevar a cabo estudios de hidrogeología y geotecnia para diseñar medidas de estabilización permanentes. Este estudio provee de parámetros geomecánicos para diseñar un sistema de protección contra caída de rocas como medida de estabilización para fallos controlados por las familias de discontinuidades.

Palabras Claves

Talud rocoso, índice de Resistencia Geológico (GSI), Análisis Cinemático, Equilibrio – Límite.

ABSTRACT

Road-cut-slope landslides are problems that cause infrastructure damage and fatalities around the world. Here, we assess the stability of 14 rock slopes in the Tena – Baeza road section. The study area lies in the subandean zone of Ecuador, an area with hilly relief and heavy rainfall, igneous and sedimentary lithological units. We use two analysis techniques: global slope stability in Slide 2D and kinematic analysis in Dips software. We computed the safety factors in Slide 2D using two Limit Equilibrium Methods (Bishop simplified and Spencer) and three saturation conditions (dry, 50% saturated and completely saturated). Furthermore, pseudostatic conditions were considered in the analysis to account for the influence of seismic activity on global stability. Kinematic analysis showed that 11 rock slopes were unstable under completely saturated conditions. In addition, these slopes have potential of wedge and planar failures. Saturated water table was the main triggering factor for instability in the studied road section. Seismic activity did not decreased the safety factors. Moreover, low Geological Strength Index values indicates that weathering and tectonism were responsible for the poor quality of rock masses. For rock slopes globally unstable, we recommend carrying out hydrogeological, geological and geotechnical studies for each slope to implement stabilization measures and refine the geological-geotechnical model of the study area. In addition, this study provides geomechanical input parameters to design a rockfall protection system as a stabilization measure for potential failure modes controlled by joint sets.

Keywords

Rock slope, Geological Strength Index (GSI), Kinematic Analysis, Limit equilibrium method.

Rock Slope Stability Analysis in a Tena – Baeza road section, Subandean Region of Ecuador

Anderson Ocampos[1*], Jorge Espin[1], Bryan Valencia[2]

[1] Geophysics and Geotechnics Research Group, Earth and Water Sciences Faculty, Universidad Regional Amazónica Ikiam, Muyuna kilometer 7-Napo-Ecuador.
[2] Department of Earth and Water Science, Universidad Regional Amazónica IKIAM, facultad.cs.tierrayagua@ikiam.edu.ec
* anderson.ocampos@est.ikiam.edu.ec

Abstract

Road-cut-slope landslides are problems that cause infrastructure damage and fatalities around the world. Here, we assess the stability of 14 rock slopes in the Tena – Baeza road section. The study area lies in the subandean zone of Ecuador, an area with hilly relief and heavy rainfall, igneous and sedimentary lithological units. We use two analysis techniques: global slope stability in Slide 2D and kinematic analysis in Dips software. We computed the safety factors in Slide 2D using two Limit Equilibrium Methods (Bishop simplified and Spencer) and three saturation conditions (dry, 50% saturated and completely saturated). Furthermore, pseudostatic conditions were considered in the analysis to account for the influence of seismic activity on global stability. Kinematic analysis showed that 11 rock slopes were unstable under completely saturated conditions. In addition, these slopes have potential of wedge and planar failures. Saturated water table was the main triggering factor for instability in the studied road section. Seismic activity did not decreased the safety factors. Moreover, low Geological Strength Index values indicates that weathering and tectonism were responsible for the poor quality of rock masses. For rock slopes globally unstable, we recommend carrying out hydrogeological, geological and geotechnical studies for each slope to implement stabilization measures and refine the geological-geotechnical model of the study area. In addition, this study provides geomechanical input parameters to design a rockfall protection system as a stabilization measure for potential failure modes controlled by joint sets.

Keywords

Rock slope, Geological Strength Index (GSI), Kinematic analysis, Limit equilibrium method, Ecuadorian subandean zone

1 Introduction

Rock slope instability is one of the most devasting natural hazards along highways in hilly regions around the world [1]. Causing serious social and economic problems to human mobility, infrastructural damage, injuries and fatalities [2]. For many years, landslides have been reported along the Y intersection between Narupa and Virgen de Guacamayos located in the Napo province, Ecuador (Fig. 1). This has caused direct damage to the road, road closure, and even fatalities. In fact, in 2019, a bus with passengers was impacted by rock blocks, causing 13 injuries and one fatality [3]. In rainy seasons, it is common for landslides to occur, resulting in total or partial road closure [4,5]. Therefore, analyzing and understanding rock instability is crucial to identify areas susceptible to landslides in this road section.

In rock slopes, several factors control their stability, such as water table, seismic activity and modifications of the slope geometry [6]. The rock mass contain structural features such as joints, bedding planes, folds, active and inactive geological faults [7]. Thus, unevenly oriented joints in the rock mass may cause failure in road cut slopes [8]. Often, joint intersections create potential structurally controlled failure modes, which are determined by kinematic analysis [1, 2, 6, 7].

Geomechanical classifications allow the quick and reliable assessment of rock mass quality [2]. Geomechanical results provide the parameters required for advanced stability methods, such as the Limit Equilibrium Method (LEM). A mathematical approach used to assess the stability of slopes on strongly weathered and fractured rock masses [7].

In this study, we carried out a rock slope stability analysis in the Y intersection of Narupa to Virgen de Guacamayos road section using global and kinematic stability analysis techniques. We expect to determine the rock slope instability driven by factors such as water saturation, slope height and slope inclination, seismic activity, and weathering.

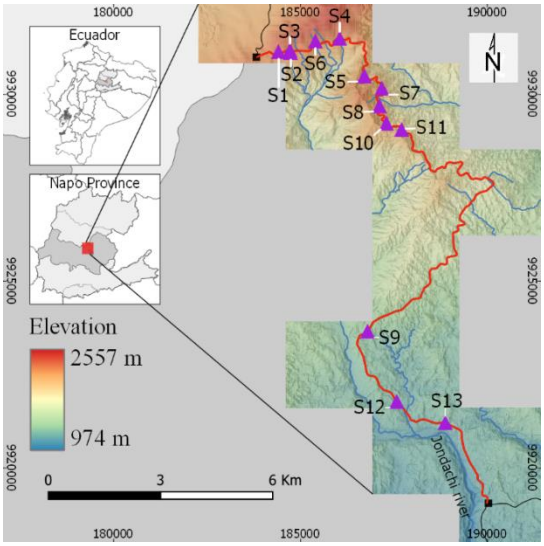

Fig. 1 Location map of the studied area. Red line is the Tena – Baeza road section, purples triangles are the rock slopes selected for stability analysis (S1 to s13). Black squares are the limits of road section, in foothill the village Y de Narupa, in the hilltop the Virgen de Guacamayos sector.

Study area

The study area is a 25-km road section located in the Ecuadorian highway E20-E45 (Fig. 1). An important motorway that connects populations in Napo province with the capital city of Ecuador. The 25 km-wide road section has been built cutting vertical slopes into the mountain that expose rock and soil profiles subjected to continuous weathering and erosion.

Most of this road is over the Guacamayos range, an east mountain belt of the Andes facing the amazon plains. The elevation range is 900 to 2250 masl, average temperature is 24º C and annual average humidity is 80% [8]. Rainfall peaks during austral summer months (June, July and August) reaching from 4000 to 5000 mm per year [8]. Overall, high rainfall, temperature and humidity promotes intense chemical weathering of the rocks in the studied area.

2.1 Geological settings

Ecuador is divided into 6 geo-structural regions from east to west [9]. The subandean zone is characterized by intense volcanic, seismic and erosive activity leading to large landslides. Our study area crosses the northern part of the Subandean region called Levantamiento Napo, a complex positive structure formed by imbricated thrust slices, and strike-slip faults with a NNE-SSW orientation [10]. The study area crosses the geological formations of the Abitagua batholith, Misahuallí formation, Hollín formation and Napo formation (Fig. 2) [11].

The Abitagua batholite is a 120 km long and 15 km wide intrusive body of NNE orientation, which forms a granitic relief of up to 2700 meters above sea level. Its compose of potassic feldspar megacrystic biotite granite to pink coarse-grained biotite monzogranite [12]. The Misahualli formation comprises the association of volcanic rocks such as trachyte, volcanic tuff, andesite, dacites and tuffaceous breccias. The Hollín formation is comprised of coarse, white and porous sandstone intercalated with dark sandy, micaceous and black carbonaceous shales. The Napo formation consists of shallow marine sandstones, claystones and limestones [12]. In addition, four Quaternary faults surround the study area. From west to east (Fig. 2), lies a dextral strike-slip fault named Rio Urcusique. From the bottom up lie the Sardinas Norte and Jondachi reverse faults. Finally, from east to west lie a strike-slip fault named Sumaco [10].

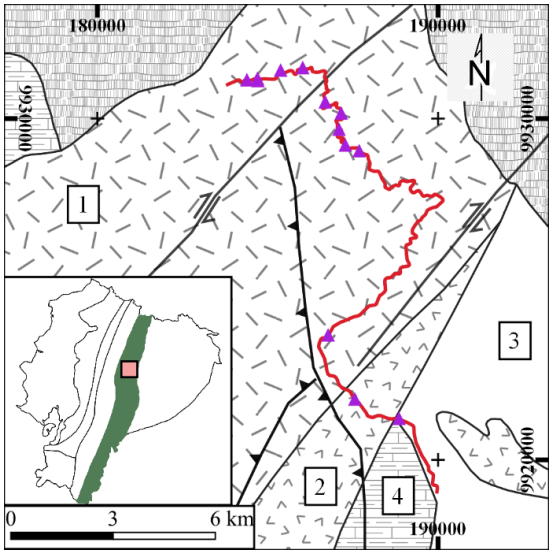

Fig. 2 Geological setting of study area. The inset in the bottom left represent the geo-structural map of Ecuador. Green shaped area is the Subandean zone. Line-arrows represent strike-slip faults and line-wedges show reverse faults. Formations were depicted by numbers, 1 Abitagua Batholith, 2 Misahualli formation, 3 Hollín formation, 4 Napo formation.

3 Methodology

Between March and June, 2021, we surveyed 13 stations where road-cut slopes were exposed along the studied road section. The stations (Table 1) were geolocated and classified based on their lithology and weathering. Because two

geomechanical surveys were performed in station S4, it was divided into stations S4_1 and S4_2 respectively (Fig. 3). We performed a visual description of the lithological texture (grain size) of the rocks outcropping at the stations. Since weathering reduces the rock strength and is a trigger for rock slope instability [13], we determined the degree of weathering of the rock mass using the Hencher and Martin classification system for granites [14] (Appendix A). This system categorizes the weathered rocks in five grades based on the rebound value of the N-type Schmidt hammer and geological observable features such as color
and texture. Thus, Grade I is for fresh rock [14], there is no visible signs of weathering or discoloration. Grade II slightly weathered, N-Schmidt hammer rebound value (RV) greater than 45. Grade III moderately weathered, $25 < RV \leq 45$. Grade IV highly weathered RV <25. Grade V completely weathered, where it is not possible to obtain a rebound value from N Schmidt hammer.

Table 1 Coordinates, exposed lithology and weathering description of studied cut rock slopes along the study area. RV is the N-type Schmidt hammer rebound value.

Station ID	Longitude	Latitude	Lithological Description	Weathering (RV)
S1	184408	9931145	Coarse-grained granite	Moderate (38)
S2	184718	9931186	Coarse-grained granite	Complete
S3	184732	9931121	Coarse-grained granite	High (20)
S4	186047	9931503	Coarse- grained granite whit mafic rock intrusions	Slight (55)
S5	186709	9930498	Fine-grained granite	Slight (56)
S6	185398	9931427	Coarse-grained granite	Moderate (37)
S7	187178	9930167	Coarse-grained granite	Moderate (39)
S8	187114	9929695	Coarse-grained granite	Moderate (43)
S9	186794	9923664	Fine-grained granite	Complete
S10	187300	9929232	Coarse-grained granite	Moderate (37)
S11	187707	9929064	Coarse-grained granite	High (23)
S12	187579	9921785	sandstone and mudstone	High (20)
S13	188875	9921219	Fine-grained sandstone and mudstone	Complete

3.1 Global Rock Slope Stability Analysis

To assess the rock mass slope stability, we used two analysis techniques: global slope stability and kinematic. To carry out the global analysis, we used the Slide 2D software [15]. This software is based on the LEM to determine the stability of a slope rock mass. LEM divides a rock mass into a finite number of vertical slices above a failure. Then, it compares the resisting and destabilizing forces on the slices to obtain a safety factor number (SF) [16]. If the SF is equal or less than one, slope failure is imminent. Conversely, SF values above 1.5 indicate that the slope is stable [17]. To define the rock mass strength, we calculated the Hoek and Brown failure criterion [18] in Slide 2D.

During fieldwork, we collected necessary parameters to determine the Geological Strength Index (GSI), Uniaxial Compressive Strength (UCS), the degree of weathering of the rock slopes, and the disturbance factor *D*. The rock constant m_i and the rock unit weight were determined from the literature [19]. We used the quantitative approach of GSI proposed by Sonmez and Ulusay (Appendix B) [20]. This approach describes the structure and properties of the rock mass to reduce subjectivity [20]. The GSI value was determined by two factors: Structure Rating (SR) and Surface Rating Condition (SRC). SR was based on the volumetric joint count (J_v) defined by Palmstrom [21] (Appendix C) and the SRC was obtained from fundamental properties of joints such as roughness (R_r), degree of weathering (R_w), thickness and fill type (R_f). Ratings for R_r, R_w, R_f were assigned according to the Rock Mass Rating system [22]. The Schmidt N-type hammer was used to obtain *in situ* rebound values of the rock mass following the methodology suggested by the International Society of Rock Mechanics ISMR [23], these values were used to obtain the UCS through the equation proposed in the Aydin and Basu study (Appendix D) [24]. The m_i value is an important parameter required for the computation of the Hoek and Brown failure criterion in estimating the strength of rock [19]. The parameter relies on the mineralogy, composition and grain size of the intact rock, and was obtained from a reference table (Appendix E) [19]. Often, blasting excavating operations, or stress relaxation disturb the rock mass structure, reducing its stability. To account for the effect of disturbance on rock mass stability, Hoek and Brown introduced the concept of the disturbance factor D. Hence, we use a value of $D = 0$ for undisturbed rock and $D = 1$ for highly disturbed rock mass [18].

We determined safety factors using Bishop and Spencer methods [16]. Bishop method assumes that the slope failure surface is of circular type, and shear forces between slices are negligible. In addition, assumes there is a vertical equilibrium of

forces for each slice and the overall moment equilibrium about the center of trial circular surface [16]. The Spencer method; however, is applicable to any type of failure surface and satisfies the equilibrium of both moments and forces in the slices. Also includes the effect of forces between slices, that allow the estimation of the safety factor [25]. Likewise, three water table conditions were consider for the computation of the safety factors. This allowed us to compare slope stability between dry conditions (no water table on the slope), slope with 50% saturated water table and slope with completely saturated water table. Similarly, we applied a stability analysis under pseudostatic conditions, to take into account the effects of earthquake shaking on slope stability. For this purpose, we computed the vertical and horizontal seismic load components following methodology suggested by the Ecuadorian Building Standard (Appendix F) [26] and we determined the maximum ground acceleration in the study area from the seismic hazard zonification map for Ecuador published in the study of Beauval et al. [27].

3.2 Kinematic Analysis

Structurally controlled stability analysis was carried out using kinematic analysis in Dips software [28]. Kinematic analysis is a geometric tool that estimates the potential failure modes in a rock mass as a function of the rock slope [1].

Moreover, kinematic analysis is usually carried out with the stereographic projection technique to determine critical zones of planar or wedge sliding occurrence [1, 2, 6]. The stereographic projection was estimated in Dips software to estimate parameters such as join sets, slope face orientation, friction angle and lateral limits on a stereonet plot. Structural data were collected in the field using a Brunton compass. For rock slope engineering, angles between 20 to 30 degrees were accepted as lateral limits [29]. The friction angle was determined using non-linear Barton – Bandis failure criterion [30], depicted in the Equation (1). Where τ is the shear strength, σ_n is the normal stress. JRC is the joint roughness coefficient and JCS is the joint compression strength.

$$\tau = \sigma_n \tan\left(\phi_r + \text{JRC}\ log_{10}\left(\frac{\text{JCS}}{\sigma_n}\right)\right) \quad (1)$$

The residual friction angle ϕ_r, was obtained by the Equation (2) [31].

$$\phi_r = (\phi_b - 20) + 20(r/R) \quad (2)$$

Where ϕ_b is the basic friction angle, its value depends on the rock type and were estimated using the tables show in Appendix H [17]. The rebound numbers *r* and *R* were obtained using the Schmidt hammer on the joint wall surface and the surface of fresh rock respectively. The joint roughness coefficient JRC was estimated by comparing the appearance of a discontinuity surface, determined by Barton`s comb, with standard profiles published by Barton and Bandis [30]. Thus, values of JRC = 0 – 2 indicate a smooth joint surface, while JRC = 18 – 20 indicate a very rough surface. The JRC parameter measures the geometric irregularities of the rock surface that produce sliding between rock blocks [32]. Generally, the rock mass joints govern the shear behavior. Therefore, determining the shear strength of discontinuities is crucial to estimate the probability of rock sliding [33]. One way to determine the joint shear strength is through the estimation of the joint wall compressive strength (JCS); we estimated this parameter using the equation proposed in the Aydin and Basu study (Appendix C) [24].

4 Results

4.1 Safety Factors using static and pseudostatic limit equilibrium methods

To compute the safety factors in Slide 2D, input parameters (Table 2) such as slope height and slope angle were used to estimate the geometric model; unit weight, GSI, UCS, m_i and *D* values to define the strength properties of the rock mass. Likewise, we entered the horizontal (Eh) and vertical (Eh) seismic load to carry out the analysis in pseudostatic conditions.

The SF for rock slopes was calculated for dry, 50% saturated and completely saturated water table conditions. Table 3 and 4 show the SF values we obtained from the Slide 2D software in static and pseudostatic conditions, respectively.

Table 2 Input parameters used in Slide 2D of studied rock slopes. SH, slope height, SA slope angle, UW rock unit weight.

ID	Parameters								
	SH (m)	SA (°)	UW (KN/m^3)	GSI	UCS (KPa)	m_i	D	Eh	Ev
S1	8	56	26	39	2000	32	0	0,022	0,014
S2	7	80	26	35	3000	32	0	0,022	0,014
S3	8	86	26	42	4000	32	0	0,022	0,014
S4-1	4	66	22	23	22000	25	0,8	0,022	0,014
S4-2	7	60	26	30	40000	32	1	0,022	0,014
S5	9	58	26	35	49000	32	0	0,022	0,014
S6	11	86	26	21	13000	32	0	0,022	0,014
S7	11	84	26	28	14000	32	0	0,022	0,014
S8	9	65	26	43	19000	32	0	0,022	0,014
S9	5	77	26	23	2000	29	0	0,029	0,019
S10	10	74	26	35	14000	32	0	0,022	0,014
S11	17	62	26	33	6000	32	0	0,022	0,014
S12	8	48	22	37	4000	22	0	0,029	0,019
S13	10	69	22	37	2000	22	0	0,029	0,019

Table 3 Estimation of SF values for rock slopes at different water table conditions (WTC) using the Bishop simplified (BPS) and Spencer (SPE) limit equilibrium methods.

ID	WTC	Safety Factors		ID	WTC	Safety Factors	
		BPS	SPE			BSH	SPE
S1	Dry	2,35	2,34	S7	Dry	2,27	2,26
	50%	2,09	2,10		50%	1,24	1,23
	Saturated	0,34	0,76		Saturated	0,15	0,51
S2	Dry	1,51	1,52	S8	Dry	4,23	4,27
	50%	0,81	0,84		50%	3,02	3,21
	Saturated	0,11	0,41		Saturated	1,24	1,71
S3	Dry	1,62	1,66	S9	Dry	1,34	1,34
	50%	0,70	0,83		50%	0,93	0,95
	Saturated	0,13	0,19		Saturated	0,09	0,53
S4_1	Dry	1,96	1,95	S10	Dry	2,69	2,72
	50%	1,28	1,30		50%	1,58	1,63
	Saturated	0,09	0,53		Saturated	0,20	0,83
S4_2	Dry	2,21	2,21	S11	Dry	2,12	2,10
	50%	1,51	1,54		50%	1,55	1,59
	Saturated	0,20	0,74		Saturated	0,11	0,64
S5	Dry	5,37	5,43	S12	Dry	3,00	3,01
	50%	4,39	4,40		50%	2,23	2,27
	Saturated	2,49	2,54		Saturated	1,21	1,31
S6	Dry	1,49	1,53	S13	Dry	1,60	1,60
	50%	1,49	1,53		50%	0,10	0,20
	Saturated	0,11	0,13		Saturated	0,10	0,20

Table 4 Estimation of SF values for rock slopes at different water table conditions under pseudostatic conditions

ID	WTC	Safety Factors		ID	WTC	Safety Factors	
		BPS	SPE			BPS	SPE
S1	Dry	2,27	2,27	S7	Dry	2,21	2,26
	50%	2,02	2,03		50%	1,22	1,26
	Saturated	0,23	0,76		Saturated	0,15	0,45
S2	Dry	1,47	1,49	S8	Dry	4,10	4,14
	50%	0,78	0,83		50%	2,92	3,09
	Saturated	0,11	0,15		Saturated	1,21	1,67
S3	Dry	1,57	1,60	S9	Dry	1,27	1,27
	50%	0,84	0,91		50%	0,90	0,94
	Saturated	0,13	0,45		Saturated	0,09	0,47
S4_1	Dry	1,90	1,90	S10	Dry	2,61	2,65
	50%	1,21	1,27		50%	1,53	1,60
	Saturated	0,09	0,59		Saturated	0,15	0,82
S4_2	Dry	2,13	2,14	S11	Dry	2,05	2,04
	50%	1,45	1,46		50%	1,50	1,56
	Saturated	0,17	0,73		Saturated	0,10	0,62
S5	Dry	5,20	5,25	S12	Dry	2,85	2,86
	50%	4,06	4,06		50%	2,03	2,08
	Saturated	2,41	2,47		Saturated	1,15	1,25
S6	Dry	1,47	1,46	S13	Dry	1,50	1,60
	50%	1,47	1,46		50%	0,10	0,30
	Saturated	0,12	0,14		Saturated	0,07	0,23

Figure 3 shows the studied rock slopes that have SF less than 1 in both static, pseudostatic and completely saturated conditions.

4.2 Kinematic Analysis of rock slope sections

Kinematic analysis was conducted using the parameters depicted in Table 5. The failure modes of the rock masses were depicted in Table 6.

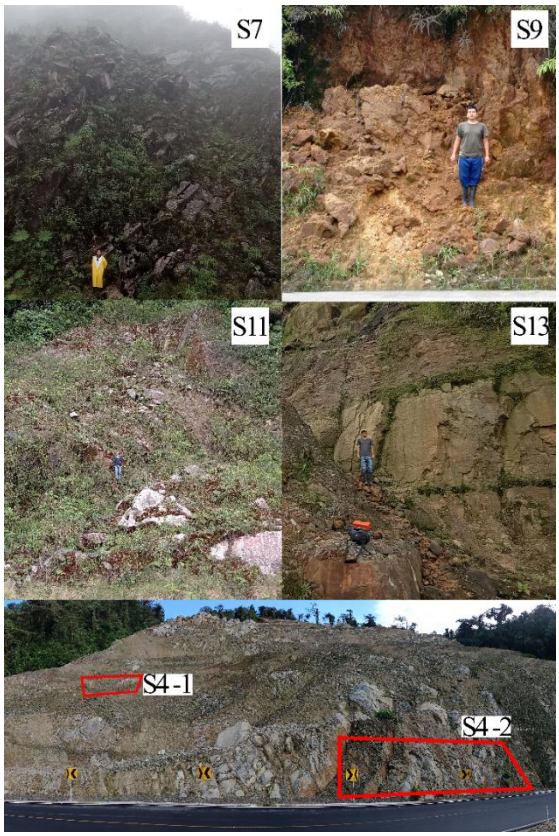

Fig. 3 Some of studied rock slopes along Y intersection of Narupa to Virgen de Guacamayos road section with safety factors less than one under completely saturated conditions.

Table 5 Input structural data to carry out the kinematic analysis; phi is the computed friction angle.

ID	Orientation (dip/dip direction)						phi
	Slope	Joint sets					
		J1	J2	J3	J4	J5	
S1	56º/254º	65º/315º	75º/221º	32º/005º			19
S2	80º/235º	28º/202º	36º/272º	2º/228º	85º/190º		28
S3	86º/257º	82º/236º	61º/190º	54º/310º	75º/295º		22
S4.1	66º/147º	38º/162º	75º/119º	89º/235º	4º/163º		38
S4.2	60º/185º	87º/153º	44º/223º	89º/113º	48º/030º	35º/290º	33
S5	58º/103º	59º/092º	88º/139º	41º/186º	86º/089º	50º/070º	32
S6	86º/078º	40º/071º	76º/336º	53º/259º	7º/235º		32
S7	84º/110º	30º/199º	57º/055º	75º/078º	89º/184º		33
S8	65º/048º	85º/086º	62º/330º	47º/057º			31
S9	77º/139º	45º/208º	89º/141º	33º/176º	84º/106º		28
S10	74º/067º	31º/040º	45º/125º	61º/057º	65º/078º		32
S11	62º/053º	26º/352º	79º/319º	81º/023º	79º/056º		35
S12	48º/232º	83º/125º	33º/195º				26
S13	69º/190º	70º/252º	87º/173º	5º/155º			23

Table 6 Causative joint sets of failure modes in rock slopes.

Station ID	Mode of failure
S1	No failure
S2	Wedge (J2-J4)
S3	Planar (J1), Wedge (J1-J3, J1-J4, J2-J3, J2-J4)
S4-1	Planar (J1)
S4-2	Wedge (J2-J3)
S5	Wedge (J1-J3)
S6	Planar (J1), Wedge (J1-J2)
S7	Wedge (J2-J4, J3-J4)
S8	Planar (J3), Wedge (J2-J3)
S9	Wedge (J1-J3, J1-J4, J3-J4)
S10	Planar (J3, J4), Wedge (J2-J3, J3-J4)
S11	No failure
S12	Wedge (J1-J2)
S13	No failure

Figures 4-6 show mixed types of failure modes found in stations S3, S6 and S10. Red dots represent the critical vector pole for planar sliding. Blue dots are the critical joint sets intersections for wedge sliding. The yellow line is the slope plane. Trend/plunge angles of intersections lines were arbitrary assigned (red number).

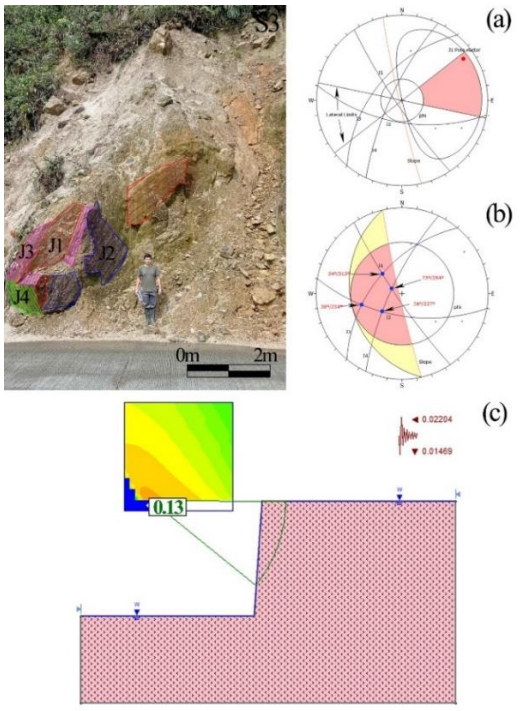

Fig. 4 Kinematic analysis for planar and wedge sliding of rock slope S3 and joint planes identified in fieldwork surveys. (a) Results of kinematic analysis for planar sliding, (b) result of kinematic analysis for wedge failure, (c) graphical output of the global stability analysis.

5 Discussion

We found that safety factors were greater than 1.5 in dry conditions for all stations, except for S9 (Tables 3, 4). However, the safety factor decreased dramatically by up to 95% under water table saturated conditions. Consequently, under saturated conditions, all the SF values were below one, except for stations S5, S8 and S12. The results indicate that the main instability factor water table

saturation. This suggest that rock slopes can fail during heavy rainfall seasons, when the water table rises. Similar results reported in a slope stability assessment along a road section in India [2]. On the other hand, kinematic analysis evidence at least one failure mode in 11 of the 14 rock slopes analyzed. The most common type wedge sliding (70%) and mixed failure modes (Table 6). Planar

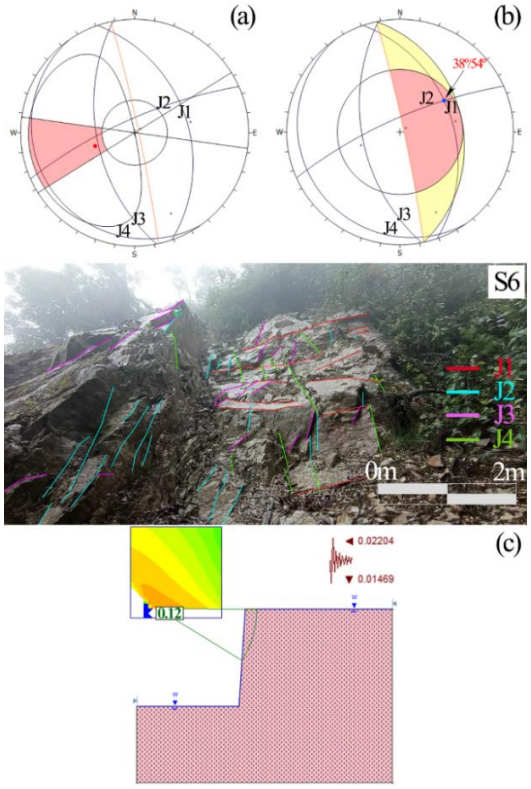

Fig. 5 Kinematic analysis for planar and wedge sliding of rock slope S6 and joints sets identified in fieldwork surveys. (a) Results of kinematic analysis for planar sliding, (b) result of kinematic analysis for wedge failure, (c) graphical output of the global stability analysis.

failure was uncommon [6]. Our results suggest that rock fall is a likely hazard for humans and infrastructure. This is consistent with rock fall events that have caused damage to vehicles, and casualties. Although we found five join sets in slopes S4_2 and S5 (Table 5), those only presented one critical intersection for wedge sliding. However, stations S3, S9 and S10, had four join sets and presented mixed failure modes.

Rock slopes with lower angle and height (Table 2) had safety factors above 1.5 as observed in S1, S4_1, S4_2, S5, S8, S10 and S12.

The percentage differences between safety factors obtained in static and pseudostatic conditions does not exceed 10%. The completely weathered rock masses, stations S2, S9 and S13 (Table 1) showed the lowest values of UCS (Table 2) and JCS (Appendix C). Conversely, slightly weathered rock masses at stations S4_1, S4_2 and S5, showed the highest UCS and JCS values. Therefore, weathering reduces the compressive strength of the rock mass. This observation is supported by the conclusions of Viles [13].

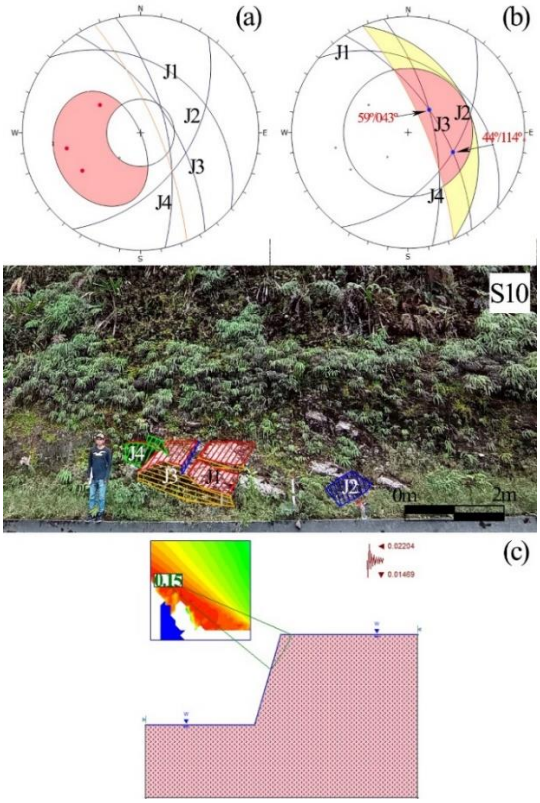

Fig. 6 Kinematic analysis for planar and wedge sliding of road cut slope S10 and joint planes identified in fieldwork surveys. (a) Results of kinematic analysis for planar sliding, (b) result of kinematic analysis for wedge failure, (c) graphical output of the global stability analysis.

Some observations in this study are worth noting. In the field surveys, we found slopes of more than 10 meters high, and slope angles greater than 70º, as in stations S3, S6, S7 and S11. USC values are dissimilar across stations although the lithology remains the same (plutonic rocks). Visually, the rock mass structure in several slopes has not been disturbed by excavations or blasting techniques,

excepting stations S4-1 and S4-2, where the disturbance factors D are equal to 0.8 and 1, respectively. The seismic load components were calculated from the wave velocity V_s of the rock profiles found in the slopes. The V_s values were obtained from literature references; Schön [34] shows the range of s-wave velocities for different common rocks such as granite, andesite, and sandstone. Similarly, Sun et al. [35] determined a range of shear wave velocities for completely weathered granitic rock layers in South Korea. Table 9 in Appendix E shows the values that we used in this study.

In addition, GSI values below 35 showed poor quality rock masses in 9 slopes. In this regard, J_v values from 10 to 30 points were found in 10 stations, this indicate a high degree of jointing [21]. In addition, the join surface condition was rated as poor, having weathered surfaces filled with soft clays [20].

By far, the hydrogeology of the zone was the main conditioning factor influencing rock slope instability. Water has several effects on the slopes, such as decreased resistance of slope failure surfaces, increased forces exerted on the tensile cracks that favor landslides; increased the weight of the rock due water saturation, erosion and physicochemical weathering leading to mineralogical changes in the rock [17]. Precipitation or runoff water increase interstitial pressure in the discontinuities, reducing effective stress and raising the probability of sliding [36]. Landslides increase during months June, July and August when rainfall reaches peaks from 4000 to 5000 mm per year [8]. Landslides in granitic rocks depend on climate decomposition factors and the erosional rock history [37]. Humid tropical climates further promote intense chemical weathering on granitic rocks, reducing the rock strength as weathering progresses [37]. Likewise, weathering and rock moisture influence the rebound value of the Schmidt hammer (hence, the UCS value) [23]. Weathering reduces rebound values nonlinearly as the moisture content increases producing microstructural changes, especially in coarse-grained igneous rocks [24]. Related to GSI values, weathering and tectonism influence the rock quality designation. Marinos [38] showed that the joint condition in slightly and moderately weathered rock mass produces a right shift in the GSI chart (fair to poor). In moderately and completely weathered rock, the joint surface condition has a poor to very poor quality designation. Likewise, GSI values are reduced in tectonic zones, especially in those experiencing a compressional tectonic regime. This ances the rock mass fractures (more joint sets) [38]. Structural maps and fault kinematic indicators show a transpressional tectonics with dextral movements in the study region and along the Subandean zone [10]. In addition, it is important to note that stress relaxation processes at the surface produce joints in the rock, which were arranged subparallel to the topographic relief and therefore the frequency of joints decrease at depth [17]. This could explain the presence of several joint sets with poor surface condition observed in the field. In addition, Brideau et al. [39] mentions that a fault damage zone tends to form an anisotropic weak rock mass from meters to tens of meters wide. In addition, their results reported that low GSI values outline tectonic damage zones.

Although the rebound value is the most practical mechanical index for estimating UCS in field, laboratory test on rock samples is required to determine strength properties, degree of weathering and moisture content [24]. However, our result remain consistent with field observations occurrence of landslides and rock falls in studied area. Further research should focus on determining the hydrogeological behavior of the materials, presence and disposition of water table, piezometric levels and water flow in rock slopes to estimate rock mass failure.

6 Conclusions and recommendations

Our study identified eleven unstable rock slopes under saturated conditions using the Bishop and Spencer methods. The study shows that increasing water tables generate instability in meteorized rocks. Chemical weathering (easily noticeable in all slopes) reduced the strength properties of the rock mass. Rock slopes stations S2, S3, S9 and S13 are unsafe under partially (50%) and saturated conditions and require inmediate slope stabilization. Stations S1, S4_1, S4_2, S6, S7, S10 and S11 are unstable in saturated conditions and are the second priority group requiring stabilization. It is important to note that in the study area, seismic activity has no influence on the

global stability of rock slopes. However, the study area is close two active seismic nests: Pisayambo and Puyo. 45 seismic events with magnitude greater than 4.5 have been detected from 1963 to 1991 in the Pisayambo nest [40]. In Puyo seismic nest, earthquakes of magnitude 4.8 to 7.1 have been detected [41]. Therefore, it is necessary to include seismic activity in the stability analysis.Kinematic analysis, shows that stations S3, S9 and S10 have a high potential for wedge failure, also planar failure was found in stations S3, S4_1, S6, S8 and S10, there is not toppling failure.

Based on the results of global and kinematic analysis, the following stabilization measures are recommended. In the case of globally unstable slopes, we recommend that specific hydrometeorological, geological and geotechnical studies be carried out for each slope to implement stabilization measures and refine the geological-geotechnical model of the study area. For rock slopes with structurally controlled but globally stable failure modes (S5, S8 and S12), we recommend the design of a rockfall protection system carrying out a slope surface coating with steel grids or rockfall netting.

Acknowledgement

We thank the company Geoprospecting for the equipment to take rock data during fieldwork surveys. We would also like to thank our university colleagues for their logistical support.

References

[1] Sarkar, K., Singh, A. K., Niyogi, A., Behera, P. K., Verma, A. K., & Singh, T. N. "The assessment of slope stability along NH-22 in Rampur-Jhakri Area, Himachal Pradesh", Journal of the Geological Society of India, 88(3), pp. 387–393, 2016. https://doi.org/10.1007/s12594-016-0500-z

[2] Anbazhagan, S., V. Ramesh, and S. E. Saranaathan. "Cut Slope Stability Assessment Along Ghat Road Section of Kolli Hills, India", Natural Hazards, 86(3), pp. 1081–1104, 2006. https://doi.org/10.1007/s11069-016-2731-0

[3] The Trade "Giant boulders fell on an interprovincial bus on the Baeza – Tena highway; one person dead and 13 injured", [online] Available at: https://www.elcomercio.com/actualidad/ecuador/rocas-deslizamiento-bus-interprovincial-fallecido.html [Accessed: 28 Dec 2019].

[4] The Trade "The Tena-Baeza road was reopened after cleanup works due to a landslide", [online] Available at: https://www.elcomercio.com/actualidad/ecuador/via-tena-baeza-habilitacion-deslizamiento.html [Accessed: 29 Oct 2020].

[5] The Trade "Baeza – Tena road partially reopened after landslide", [online] Available at: https://www.elcomercio.com/actualidad/ecuador/via-tena-baeza-habilitacion-deslizamiento.html [Accessed: 29 Dec 2019].

[6] Sardana, S., Verma, A. K., Verma, R., & Singh, T. N. "Rock slope stability along road cut of Kulikawn to Saikhamakawn of Aizawl, Mizoram, India", Natural Hazards, 99(2), pp. 753–767, 2019. https://doi.org/10.1007/s11069-019-03772-4

[7] Zhang, K. "Failure Mechanism and Stability Analysis of rock slopes", Springer Singapore, Singapore, 2020. https://doi.org/10.1007/978-981-15-5743-9

[8] Municipality of Archidona. "Development and land use plan", Municipality of Archidona, Archidona, Ecuador, Rep. 1, 2014.

[9] Aspden, J. A., & Litherland, M. "The geology and Mesozoic collisional history of the Cordillera Real, Ecuador", Tectonophysics, 205(1-3), pp. 187–204, 1992. https://doi.org/10.1016/0040-1951(92)90426-7

[10] Baby, P., Rivadeneira, M., Barragán, R. "La cuenca Oriente: geología y petróleo", Institut français d'études andines, Lima, Perú, 2004. https://doi.org/10.4000/books.ifea.2971

[11] Balseca, W., Ferrari, L., Pasquare, G., Tibaldi, A. "Structural evolution of the Northern Sub-Andes of Ecuador: The Napo Uplift", In: International Symposium on Andean Geodynamics (ISAG), Oxford, United Kingdom, 1993, pp. 163-166.

[12] Ruiz, R. "Exhumation of the northern Sub-Andean Zone of Ecuador and its source regions a combined thermochronological and heavy mineral approach", Doctoral Thesis, Swiss Federal Institute of Technology in Zürich, 2002. [online] Available at: https://doi.org/10.3929/ethz-a-004489528

[13] Viles H. "Linking weathering and rock slope instability: non-linear perspectives", Earth Surface Processes and Landforms, 38(1), pp.62-70, 2012. https://doi.org/10.1002/esp.3294

[14] Hencher S.R., Martin R.P. "The description and classification of weathered rocks in Hong Kong for engineering purposes", In: Proceedings of 7th South-east Asian Geotechnical Conference, Hong Kong, China, 1982, pp.125-142.

[15] Rocscience "Slide 2D 9.017", [computer program] Available at: https://www.rocscience.com/software/slide2 [Accessed: 14 5 2021].

[16] Abramson, L.W., Lee, T.S., Sharma, S., Boyce, G. "Slope Stability and Stabilization Methods", John Wiley & Sons.

[17] Gonzales de Vallejo L., Ferrer M., Ortuño L., Oteo C. "Ingeniería Geológica", Pearson Educación, Madrid, España, 2002.

[18] Hoek, E., Carranza, C., Corkum, B. "Hoek-Brown Failure Criterion – 2002 Edition", In: North American Rock Mechanics Symposium, Toronto, Canada, July 10, 2002.

[19] Hoek E., Kaiser P.K., Bawden W.F. "Support of underground excavations in hard rock", A.A. Balkema, Rotterdam, Netherlands, 1995.

[20] Sonmez, H., Ulusay, R. "Modifications to the geological strength index (GSI) and their applicability to stability of slopes", International Journal of Rock Mechanics and Mining Sciences, 36(6), pp. 743–760, 1999. https://doi.org/10.1016/s0148-9062(99)00043-1

[21] Palmstrom, A. "Measurements of and correlations between block size and rock quality designation (RQD)", Tunnelling and Underground Space Technology, 20(4), pp. 362–377, 2005. https://doi.org/10.1016/j.tust.2005.01.005

[22] Bieniawski Z.T. "Engineering rock mass classifications", John Wiley & Sons, New York, United States of America, 1989.

[23] Ulusay, R. "The ISRM Suggested Methods for Rock Characterization, Testing and Monitoring: 2007-2014", Springer International Publishing, Switzerland, 2015. https://doi.org/10.1007/978-3-319-07713-0

[24] Aydin A., Basu A. "The Schmidt hammer in rock material characterization", Engineering Geology, 81(1), pp-1-14, 2005. http://dx.doi.org/10.1016/j.enggeo.2005.06.006

[25] Abdallah, I., Malkawi, H., Hassan, W., Fayez, A. "Uncertainty and reliability analysis applied to slope stability", Structural Safety, 22(2), pp. 161-187, 2000. http://dx.doi.org/10.1016/s0167-4730(00)00006-0

[26] Ministry of Urban Development and Housing "Seismic Hazard Seismic Resistant Design", [pdf] Social Communication Department MIDUVI, Available at: https://www.habitatyvivienda.gob.ec [Accessed: 14 7 2021].

[27] Beauval, C., Marinière, J., Yepes, H., Audin, L., Nocquet, J.M., Alvarado, A., Baize, S., Aguilar, J., Singaucho, J., Jomard, H. "A new Seismic Hazard Model for Ecuador", Bulletin of the Seismological Society of America, 108(3), pp.1443-1646, 2018. https://doi.org/10.1785/0120170259

[28] Rocscience "Dips 8.013", [computer program] Available at: https://www.rocscience.com/software/dips [Accessed: 14 5 2021].

[29] Sikveland, G. "A structural, geomorphological and InSAR study of unstable rock slopes at Mellomfjellet, Nordreisa", Master Thesis, The Arctic University of Norway, 2019. [online]. Available at: https://munin.uit.no/handle/10037/15413

[30] Barton, N., Bandis, S. "Review of predictive capabilities of JRC-JCS model in engineering practice", In: International Symposium on Rock Joints, Loen, Norway, 1990, pp. 603-610.

[31] Barton, N., Choubey, V. "The shear strength of rock joints in theory and practice", Rock Mechanics Felsmechanik Mecanique des Roches, 10(1), pp. 1–54, 1977. https://doi.org/10.1007/bf01261801

[32] Tse R., Cruden D. "Estimating joint roughness coefficients", International Journal of Rock Mechanics and Mining Science & Geomechanics Abstracts, 16(5), pp. 303-307, 1979. https://doi.org/10.1016/0148-9062(79)90241-9

[33] Du S., Hu Y., Hu X., Guo X. "Comparison between empirical estimation by JRC-JCS model and direct shear test for joint shear strength", Journal of Earth Science, 22(3), pp. 411-420. https://doi.org/10.1007/s12583-011-0193-6

[34] Schon, J.H. "Physical Properties of Rocks", Elsevier, Oxford, United Kingdom, 2011.

[35] Sun, C.-G., Kim, B.-H., Park, K.-H., & Chung, C.-K. "Geotechnical comparison of weathering degree and shear wave velocity in the decomposed granite layer in Hongseong, South Korea", Environmental Earth Sciences, 74(9), pp. 6901–6917, 2015. https://doi.org/10.1007/s12665-015-4692-0

[36] Guglielmi, Y., Cappa F., Rutqvist, F., Tsang C-F., Thoraval, A. "Field and numerical investigations of free-water surface oscilation effects on rock slope hydromechanical behavior consequences for rock slope stability analyses", In: GEOPROC 2006 International Symposium, Nanjing, China, 2006, pp.1-2.

[37] Durgin, P. "Landslides and the weathering of granitic rocks", Reviews in Engineering Geology, pp. 125–132, 1977. https://doi.org/10.1130/reg3-p125

[38] Marinos, V. "Applications of the GSI system to the classification of soft rocks", In: Kanji, M., He, M., & Ribeiro e Sousa, L. (eds.) Soft rock mechanics and engineering, Springer Nature Switzerland, Cham, Switzerland, 2020, pp. 503-541. https://doi.org/10.1007/978-3-030-29477-9

[39] Brideau, M.-A., Stead, D., Kinakin, D., & Fecova, K. "Influence of tectonic structures on the Hope Slide, British Columbia, Canada", Engineering Geology, 80(3-4), pp. 242–259, 2005. https://doi.org/10.1016/j.enggeo.2005.05.004

[40] Aguilar, J., Chatelain, J.L., Guillier, B., Yepes, H. "The Pisayambo, Ecuador, Seismicity Nest: Towards the Birth of a Volcano", In: Third International Symposium on Andean Geodynamics (ISAG), Paris, France, 1996, pp.125-128.

[41] Moncayo, G. A., Monsalve, G., & Zuluaga, J. I. "Tidal Coulomb Failure Stresses in the northern Andean intermediate depth seismic clusters: Implications for a possible correlation between tides and seismicity". Tectonophysics, 762, pp. 61–78, 2019. https://doi.org/10.1016/j.tecto.2019.04.015

Appendix

Appendix A – Geological Strength Index (GSI) values

Table 7 Input parameters used to determine the GSI value and rock mass rating

Station ID	Parameters							
	Roughness Rating (R_r)	Weathering Rating (R_w)	Infilling Rating (R_f)	Volumetric joint count (J_v)	SR = $-17.5ln(J_v) + 78.9$	SCR = $R_r + R_w + R_f$	GSI	Description
S1	3	1	6	17.37	29.84	10	39	Poor rock
S2	0	1	6	10.04	39.44	7	35	Poor rock
S3	2	5	2	8.95	41.45	9	42	Fair rock
S4-1	2	0	2	24.45	23.86	4	23	Poor rock
S4-2	2	2	2	16.53	30.71	6	30	Poor rock
S5	5	1	2	18.34	28.89	8	35	Poor rock
S6	2	0	2	28.27	21.32	4	21	Poor rock
S7	2	0	0	4.08	55.19	2	28	Poor rock
S8	4	2	3	7.54	44.44	9	43	Fair rock
S9	3	0	0	14.26	33.29	3	23	Poor rock
S10	5	0	2	11.79	36.62	7	35	Poor rock
S11	2	0	1	3.54	57.69	3	33	Poor rock
S12	5	0	2	28.63	21.1	7	37	Poor rock
S13	6	0	2	10.07	39.38	8	37	Poor rock

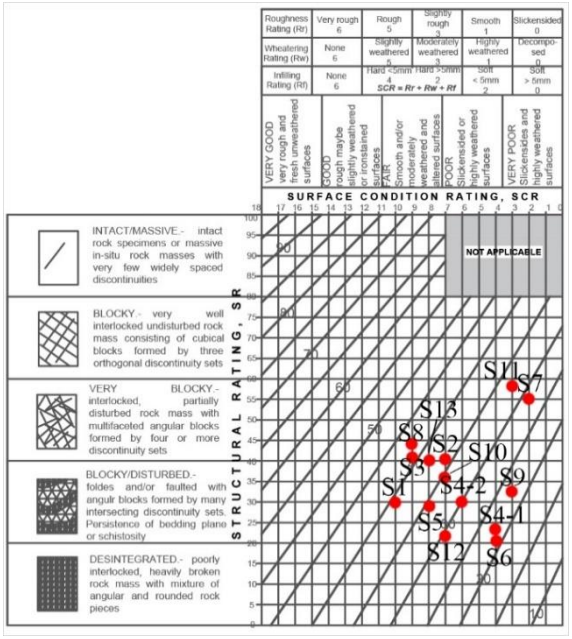

Fig. 7 GSI values plotted in the modified GSI chart by Sonmez and Ulusay [17].

Appendix B – Joint Volumetric count (J_v)

Palmstrom [21] defines the joint volumetric count with the following equation.

$$J_v = 1/S_1 + 1/S_2 + 1/S_3 + \cdots 1/S_n \quad (3)$$

Where $\boldsymbol{S_1}$, $\boldsymbol{S_2}$ and $\boldsymbol{S_3}$ are the average spacings for *n* joint sets.

Appendix C – Uniaxial Compressive Strength (UCS)

Aydin and Basu [24] propose the following equation to obtain the Uniaxial Compressive Strength from the rebound values of the Schmidt hammer. This ration is suitable for granitic rocks.

$$UCS = 1.45 \times e^{(0.07 * R_N)} \quad (4)$$

Where R_N is the rebound value for N-type Schmidt hammer.

Appendix D - m_i values and rock unit weight

Hoek, Kaiser and Bawden [19] compile in their study a table of the m_i values for intact rocks based on rock type, class and texture. Table 8 shows the values we used in this study. We took of the rock unit weight from the book by Gonzales de Vallejo et al. [17].

Table 8 Values of the rock constant $\boldsymbol{m_i}$ used in this study. CW completely weathered.

Rock type	Class	Texture	Rock	m_i	Rock unit weight (KN/m^3)
igneous	light	coarse	granite	33	26
igneous	light	coarse	CW granite	29	26
igneous	dark	fine	andesite	25	22
sedimentary	clastic	medium	sandstone	22	23

Appendix E – Computation of the horizontal and vertical seismic loads

The Ecuadorian building standard [24] proposes the following methodology to design civil engineering projects taking into account seismic loads.

First, we defined the type of soil profile from the shear wave velocity $V_s(m/s)$ for all the lithological units. Table 9 shows the values that we used in this

study. The data were obtained from the references [34, 35]. Table 10 shows the types of soil profiles according to the value of the s-wave.

Table 9 V_s values used in this study. CW completely weathered.

Rock Type	Shear wave velocity V_s (m/s)	Reference
granite	2600-3300	[34]
andesite	2400-3500	[34]
sandstone	1100-2700	[34]
CW granite	300-500	[35]

Table 10 Soil types determined in this study

Type of soil profile	Definition
A	$V_s \geq 1500\, m/s$
B	$1500\, m/s > V_s \geq 760\, m/s$
D	$360\ m/s > V_s \geq 180\, m/s$

Second, we obtained the Z zone factor 0.40, from the seismic zonation map published in the study of Beauval et al. [27]. Then, we obtained the soil amplification coefficient F_a based on soil profiles and Z (Table 11).

Table 11 Determination of the soil amplification coefficient

Type of soil profile	Z	Fa
A	0,4	0,9
B	0,4	1
D	0,4	1,2

Next, we compute the peak ground acceleration a_{max} by multiplying the zone factor and the soil amplification coefficient. The horizontal seismic load E_h was computed by the equation 5.

$$E_h = \frac{0.6 \times a_{max}}{9.8} \quad (5)$$

We calculate the vertical seismic load by scaling the horizontal component using equation 6.

$$E_v \geq \frac{2}{3} \times E_h \quad (6)$$

Thus, table 12 summarized all the input parameters that we used to calculate the seismic load.

Table 12. Input parameters to calculated the horizontal and vertical seismic loads. TSP Type of soil profile.

Station ID	Lithology	V_s (m/s)	TSP	Z	F_a	a_{max}	E_h	E_v
1	granite	2900	A	0,4	0,9	0,4	0,0220	0,0147
2	granite	2900	A	0,4	0,9	0,4	0,0220	0,0147
3	granite	2900	A	0,4	0,9	0,4	0,0220	0,0147
4.1	andesite	2900	A	0,4	0,9	0,4	0,0220	0,0147
4.2	granite	2900	A	0,4	0,9	0,4	0,0220	0,0147
5	granite	2900	A	0,4	0,9	0,4	0,0220	0,0147
6	granite	2900	A	0,4	0,9	0,4	0,0220	0,0147
7	granite	2900	A	0,4	0,9	0,4	0,0220	0,0147
8	granite	2900	A	0,4	0,9	0,4	0,0220	0,0147
9	CW granite	100-350	D	0,4	1,2	0,5	0,0294	0,0196
10	granite	2900	A	0,4	0,9	0,4	0,0220	0,0147
11	granite	2900	A	0,4	0,9	0,4	0,0220	0,0147
12	sandstone	1484	B	0,4	1	0,4	0,0245	0,0163
13	sandstone	1484	B	0,4	1	0,4	0,0245	0,0163

Appendix F – Weathering classification system

Hencher and Martin [24] propose the following classification chart for weathered granitic rocks (Table 13).

Table 13 Weathering classification system chart based in the rebound value of N-type Schmidt hammer, discoloration and geological hammer **test.**

Grade	Description	Distinctive Characteristic
V	completely weathered rock	No rebound value of Schmidt hammer. Geological hammer easily indents the rock.
IV	highly weathered rock	Rebound values up to 25. Large pieces of rock can be broken by hand.
III	moderately weathered rock	Completely discolored rock. Pieces 55mm diameter cannot be broken by hand Range rebound values from 25 to 45.
II	slightly weathered rock	Discoloration between rock mass joints. More than one blow of the geological hammer to break up the rock. Rebound values greater than 45
I	fresh rock	Absent weathering and discoloration of the rock

Appendix G – basic friction angle

Table 14 shows all the values of basic friction angle degrees used in this study [17].

Table 14 Basic friction angles in degrees

Rock	ϕ_b(degrees)
coarse grained granite	31 -33
fine grained granite	31- 35
andesite	45
sandstone	29